A new approach to enhancing the CO_2 capture performance of defective UiO-66 via post-synthetic defect exchange

Athanasios Koutsianos,[a] Ewa Kazimierska,[a] Andrew R. Barron,[a,b,c] Marco Taddei,*[a] and Enrico Andreoli*[a]

Zirconium-based metal-organic frameworks (Zr-MOFs) are a subclass of MOFs known for their remarkable stability, especially in the presence of water. This makes them extremely attractive for practical applications, including CO_2 capture from industrial emission sources; however, the CO_2 adsorption capacity of Zr-MOFs is moderate compared to that of the best performing MOFs reported to date. Functionalization of Zr-MOFs with amino groups has been demonstrated to increase their affinity for CO_2. In this work, we assessed the potential of post-synthetic defect exchange (PSDE) as an alternative approach to introduce amino functionalities at missing-cluster defective sites in formic acid modulated UiO-66. Both pyridine-containing (picolinic acid and nicotinic acid) and aniline-containing (3-aminobenzoic acid and anthranilic acid) monocarboxylates were integrated within defective UiO-66 with this method. Non-defective UiO-66 modified with linkers bearing the same amino groups (2,5-pyridinedicarboxylic acid and 2-aminoterephthalic acid) were prepared by classical post-synthetic ligand exchange (PSE), in order to compare the effect of introducing functionalities at defective sites versus installing them on the backbone. PSDE reduces the porosity of defective UiO-66, but improves both the CO_2 uptake and the CO_2/N_2 selectivity, whereas PSE has no effect on the porosity of non-defective UiO-66, improving the CO_2 uptake but leaving selectivity unchanged. Modification of defective UiO-66 with benzoic acid reveals that pore size reduction is the main factor responsible for the observed uptake improvement, whereas the presence of nitrogen atoms in the pores seems to be beneficial for increasing selectivity.

Introduction

The Committee on Climate Change (CCC) has recently released its annual report on greenhouse gases reduction progress for 2018.[1] Among the key messages of the report is the necessity to cut CO_2 emissions from industry. In contrast to the power sector, industrial emissions rose by 1% in 2017 rendering the implementation of industrial carbon capture, utilization and storage (CCUS) imperative.[1] During the last decades, post combustion capture (PCC) using liquid amines (i.e., amine scrubbing) has been used on commercial scale and it is considered to have a technology readiness level of 9.[2] According to a recent study though, PCC displays higher operation and maintenance costs than oxy-fuel and pre-combustion capture technologies.[3] The high costs are ascribed to several issues that liquid phase chemical absorption suffers from, such as equipment corrosion, high regeneration energy, solvent loss and toxicity.[4] Binding of CO_2 by solid sorbents has thus been proposed as an alternative for CCUS applications.[5] Solid amines have been extensively studied owing to their high selectivity and stability to humid conditions,[6, 7] however the energy-demanding regeneration of such materials remains a drawback. In this context, physical binding by porous polymers and metal-organic frameworks (MOFs) have drawn interest as promising sorbents, owing to their high porosity and structural and chemical versatility.[8-10] The main pitfall that so far has hindered large scale deployment of MOFs for CCS is their limited stability in working conditions.[11] In recent years, though, robust MOF structures have been emerged, with potential for capture also in humid conditions.[12-14]

Zr-based MOFs (Zr-MOFs) have lately become one intensely investigated subclass of MOFs, due to their remarkable stability, especially in the presence of water.[13] This feature makes them attractive for application in industrially relevant settings, including CO_2 capture, where the presence of water is unavoidable.[15] Unfortunately, the uptake performance of Zr-MOFs appears moderate, when compared with other MOFs,[11] and they suffer from low selectivity, a necessary feature for separation of dilute CO_2 streams in the low partial pressures regime.[16]Apart from the use of metal sites in the structures to enhance capture properties,[17] chemical modification of MOFs with nitrogen atoms has been also investigated, aiming at a more polar sorption material and the resulting enhanced dipole-quadrupole interactions between CO_2 molecules and the nitrogen sites of the sorbent.[16] Framework functionalization via direct synthesis using either linkers bearing amino functionalities or nitrogen containing heterocycles have been used and afforded enhanced affinity for CO_2 in Zr-MOFs.[18-20] This enhancement was attributed to either (a) cooperation between -NH_2 groups and -OH groups in the clusters in binding CO_2 molecules[18] or (b) presence of nucleophilic heterocyclic nitrogen species.[20] A similar trend was also displayed by Zr-MOFs where ethanolamine was post-synthetically grafted to the clusters, which led to efficient CO_2 capture by formation of

[a] Energy Safety Research Institute, Swansea University, Fabian Way, Swansea, SA1 8EN, UK. E-mail: marco.taddei@swansea.ac.uk, e.andreoli@swansea.ac.uk
[b] Department of Chemistry, Rice University, Houston, Texas, 77005, USA.
[c] Department of Materials Science and Nanoengineering, Rice University, Houston, Texas, 77005, USA

carbamate species.[21] Nitrogen functionalization was also achieved via solvent assisted ligand incorporation

The presence of structural defects in Zr-MOFs has been recently revealed and the subsequent exploitation of defects towards tuning of physical-chemical properties has drawn considerable attention.[22-25] With regard to CO_2 capture, a recent study demonstrated that monocarboxylate groups derived from crystallization modulators and grafted at the missing-cluster defective sites in the prototypical Zr-MOF UiO-66, based on 1,4-benzenedicarboxylic acid (terephthalic acid, BDC) and having ideal formula $Zr_6O_4OH_4(BDC)_6$, can be post-synthetically exchanged with *L*-serine ligands, enhancing capture capacity.[26] We recently observed that when soaked in a solution of a terephthalic acid analogue, defective UiO-66 undergoes preferential exchange of defect-compensating monocarboxylic groups rather than replacement of linker molecules constituting the framework backbone.[27] This process is termed post-synthetic defect exchange (PSDE). The textural and CO_2 sorption properties of the resulting MOFs were influenced in a different manner to when the terephthalic acid analogue was installed in the framework. These results prompted us to systematically investigate the potential of PSDE as a method for improving the CO_2 capture performance of defective UiO-66. The goal of this study was to incorporate a range of monocarboxylate species bearing nitrogen moieties within UiO-66 via PSDE, with the aim of tailoring the physical-chemical properties of the sorbent material and examine if and how the nature and orientation of the amino functional groups affect the sorption properties. Dicarboxylic linker analogues were introduced in non-defective UiO-66 by classical post-synthetic ligand exchange (PSE), in order to compare the different effects of defect functionalization and framework functionalization on the physical-chemical properties.

Experimental

Chemicals

$ZrCl_4$ (98%) and 2-amino-1,4-benzenedicarboxylic acid (ABDC, 99%) were purchased from Acros Organics. 1,4-benzenedicarboxylic acid (BDC, 98%) and benzoic acid (BA, 99%) were purchased from Alfa Aesar. Formic acid (FA, 98-100%), 2,5-pyridinedicarboxylic acid (PyDC) and anthranilic acid (AA, 99%) were purchased from Merck Millipore. *N,N*-dimethylformamide (DMF) was purchased from VWR. Nicotinic acid (NA, 99%) was provided by Sigma. 3-aminobenzoic acid and picolinic acid (PA, 99%) were purchased from Aldrich. Chemical structures of the employed carboxylic acids are provided in Figure 1.

Synthetic procedures

Defective UiO-66 synthesized in the presence of FA modulator is henceforth denoted as FA_mod. Respectively, FA_mod-XX refers to the materials prepared by PSDE method, resulting from the exchange of the FA species in the parental FA_mod with NA (thus giving FA_mod-NA), PA (thus giving FA_mod-PA), BA (thus giving FA_mod-BA), ABA (thus giving FA_mod-ABA) and AA (thus giving FA_mod-AA). Non-defective UiO-66 is named as No_mod. No_mod-XXXX denotes samples obtained after exchanging BDC linkers of No_mod with either PyDC (thus giving No_mod-PyDC) or ABDC (thus giving No_mod-ABDC) by PSE.

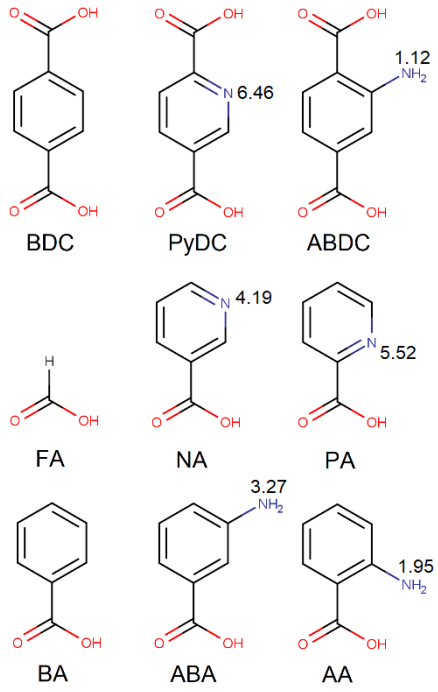

Figure 1. Chemical structures of the carboxylic acids employed in this study: terephthalic acid (BDC), 2,5-pyridinedicarboxylic acid (PyDC), 2-aminoterephthalic acid (ABDC), formic acid (FA), picolinic acid (PA), nicotinic acid (NA), 3-aminobenzoic acid (ABA), anthranilic acid (AA) and benzoic acid (BA). pKa values of the conjugate acid are shown for each amine group. The values were obtained from the online tool *Chemicalize*.

Synthesis of FA_mod. $ZrCl_4$ (1.165 g, 5.000 mmol) was dissolved in DMF (81 mL), followed by the addition of water (0.270 mL, 15.0 mmol), FA (18.8 mL, 500 mmol) and BDC (0.870 g, 5.00 mmol). The mixture was sonicated until complete dissolution, divided into ten 20 mL vials and kept for 16 hours at 120 °C. The solid was subsequently centrifuged and washed with DMF (25 mL, one-hour soaking), water (2 × 25 mL, one-hour soaking) and acetone (25 mL, one-hour soaking; 25 mL, overnight soaking). The solid was dried in air at 80 °C for two hours.

Synthesis of defect-engineered materials. FA_mod-NA, FA_mod-PA, FA_mod-BA, FA_mod-ABA and FA_mod-AA resulted from the suspension of FA_mod (500 mg) in the respective solution of NA, PA, BA, ABA and AA (0.025 M) in DMF (33 mL) for 24 hours at 80 °C. Afterwards the solids were centrifuged and washed with DMF (25 mL, one-hour soaking), water (2 × 25 mL, one-hour soaking) and acetone (25 mL, one-hour soaking; 25 mL, overnight soaking). The solids were dried in air at 80 °C for two hours.

Synthesis of No_mod. $ZrCl_4$ (1.165 g, 5.000 mmol) was dissolved in DMF (100 mL), followed by the addition of water (0.270 mL, 15.0 mmol) and BDC (0.870 g, 5.00 mmol). The mixture was sonicated until complete dissolution, divided into ten 20 mL vials and kept for 16 hours at 120 °C. The solid was subsequently centrifuged and washed with DMF (25 mL, one-hour soaking),

water (2 × 25 mL, two-hour soaking) and acetone (25 mL, one-hour soaking; 25 mL, overnight soaking). The solid was dried in air at 80 °C for two hours.

Synthesis of No_mod-PyDC. No_mod (500 mg) was suspended in a solution of PyDC (0.025 M) in DMF (33 mL) for 24 hours at 80 °C. The solid was then centrifuged and washed with DMF (25 mL, one-hour soaking), water (2 × 25 mL, two-hour soaking) and acetone (25 mL, one-hour soaking; 25 mL, overnight soaking). The solid was dried in air at 80 °C for two hours.

Synthesis of No_mod-ABDC. No_mod (500 mg) was suspended in a solution of ABDC (0.075 M) in DMF (33 mL) for 72 hours at 120 °C. The solid was subsequently centrifuged and washed with DMF (25 mL, one-hour soaking), water (2 × 25 mL, two-hour soaking) and acetone (25 mL, one-hour soaking; 25 mL, overnight soaking). The solid was dried in air at 80 °C for two hours.

Analytical procedures

Quantitative NMR analysis of hydrolyzed solids was performed with a Bruker AV-500 Avance III spectrometer. About 15 mg of solid was digested for 24 h in 1 mL of 1 M NaOH in D_2O. The NMR tubes were then loaded with the solution, which was filtered through cotton wool to avoid the presence of solid particles in dispersion.

Powder X-ray diffraction (PXRD) patterns were collected in the 4-30° 2θ range with a Bruker D8 Avance diffractometer working in reflection geometry and equipped with a LYNXEYE XE detector, using the Cu Kα radiation. The X-ray tube was operated at 40 kV and 40 mA.

N_2 sorption isotherms at 77 K were measured with a Quantachrome Nova 2000e analyzer. The samples (about 30-50 mg) were kept overnight in an oven at 100 °C, then activated for four hours under vacuum at 120 °C prior to analysis. BET surface areas were calculated in the 0.001-0.043 P/P_0 range, where all the criteria defined by Gomez-Gualdron et al.[28] were fulfilled. Micropore volume was derived using the t-Plot method in the 0.19-0.52 P/P_0 range. Pore size distribution was determined using the Density Functional theory (DFT) method implemented in the Quantachrome NovaWin software. The kernel implemented in NovaWin software was Non Local DFT (NLDFT)-N_2 - silica equilibrium transition kernel at 77 K based on a cylindrical pore model.

High pressure CO_2 and N_2 excess adsorption isotherms were measured at 283 K (CO_2), 298 K (CO_2 and N_2), 313 K (CO_2) with a Quantachrome iSorb HP1 analyser. The samples (about 150-200 mg) were activated under vacuum with a stepwise procedure keeping them at 60 °C for 1 hour, 80 °C for 1 hour and 120 °C for 4 hours. This procedure was employed in order to prevent abrupt removal of adsorbed solvents (i.e. acetone and water). CO_2 isotherms were fitted using the Dual Site Langmuir equation. N_2 isotherms were fitted using the Langmuir-Freundlich equation (dual site Langmuir-Freundlich was used for No_mod-ABDC). The isosteric enthalpy of CO_2 adsorption (IEA) was calculated by using the linear version of the Clausius-Clapeyron equation in the loading range 0.1-1.0 mmol g^{-1}. Ideal adsorbed solution theory (IAST) CO_2/N_2 selectivity for a 0.15:0.85 CO_2/N_2 mixture in the pressure range 1-5 bar was calculated using the simulated isotherms obtained from the software *IAST++*.[29]

Thermogravimetric analysis (TGA) was performed with a TA Instruments SDT-Q600 instrument using alumina cups at and a 5 °C min^{-1} heating rate up to 700 °C in air.

Scanning electron microscopy (SEM) was performed with a JEOL 7800F FEG SEM instrument with an acceleration voltage of 7.0 kV. The powders were deposited on carbon sticky tape on an aluminum support and sputtered with chromium (current: 100 mA; time: 30 s; thickness: 2 nm).

Results and discussion

Fundamental aspects of PSE and PSDE

The basic concepts of PSE and PSDE are shown in Figure 2. Both methods rely on the modification of a pristine MOF matrix (UiO-66 in this work) by exchange of carboxylic species coordinated to the metal clusters with new carboxylic species. There are substantial differences in the modifications occurring within the porous framework when it is subjected to PSE versus when it is subjected to PSDE.

PSE (Figure 2a) involves replacement of a dicarboxylic linker (BDC in this work, see Figure 1) by another dicarboxylate having the same size and bearing a functional group (PyDC or ABDC in this work, see Figure 1). The resulting mixed-linker MOF displays homogeneous distribution of functionalized linkers throughout its structure,[30] unless crystallite size is not in the 10-100 µm range, where formation of core-shell structures could be observed.[31] If the new linker does not bear bulky and heavy functional groups (as is the case of this work), no drastic changes in the porosity of the framework are expected, which allows isolation of the effect of chemical modification on the physical-chemical properties of the framework.

In the case of PSDE (Figure 2b), the exchanged species is a monocarboxylic modulator grafted at a defective site (FA in this work, see Figure 1), which can be replaced by any species containing at least one carboxylic group. Upon complete PSDE of FA, only the defective part of the framework is selectively functionalized and reduction of porosity is expected, due to crowding of the pores. As a result, PSDE has an effect on both the textural features of the MOF and the physical-chemical environment at missing-cluster defective sites. As recently demonstrated, PSE and PSDE compete when defective UiO-66 is soaked in a solution of a terephthalic acid analogue.[27] In order to have pure PSDE, we employed both bare BA and benzoic acid analogues bearing amino functionalities (i.e. PA, NA, AA and ABA, see scheme 1). The amino-functionalized monocarboxylates were selected because of their analogous nature to PyDC and ABDC, which are commonly used linkers for introducing amino functionalities in Zr-MOF frameworks, with the aim of comparing the effect of PSE and PSDE on the CO_2 capture performance. By the use of BA, we aimed at identifying the pore size engineering effect of replacing FA with BA, which has similar size to the other monocarboxylates, but does not possess any nitrogen moieties.

PSDE is a similar process to solvent assisted ligand incorporation (SALI), which has been proposed by Farha and coworkers.[32, 33] Both processes involve exchange of monocarboxylate species grafted on undercoordinated Zr clusters. SALI has been employed to functionalize the clusters of "intrinsically defective" Zr-MOF NU-1000 (featuring eight connected clusters). Different from UiO-66, functionalization of NU-1000 is only possible through SALI. We here employ the denomination PSDE because this term is more specific for proper defective MOFs and to emphasize its alternative nature to classical PSE for functionalization of Zr-MOFs.

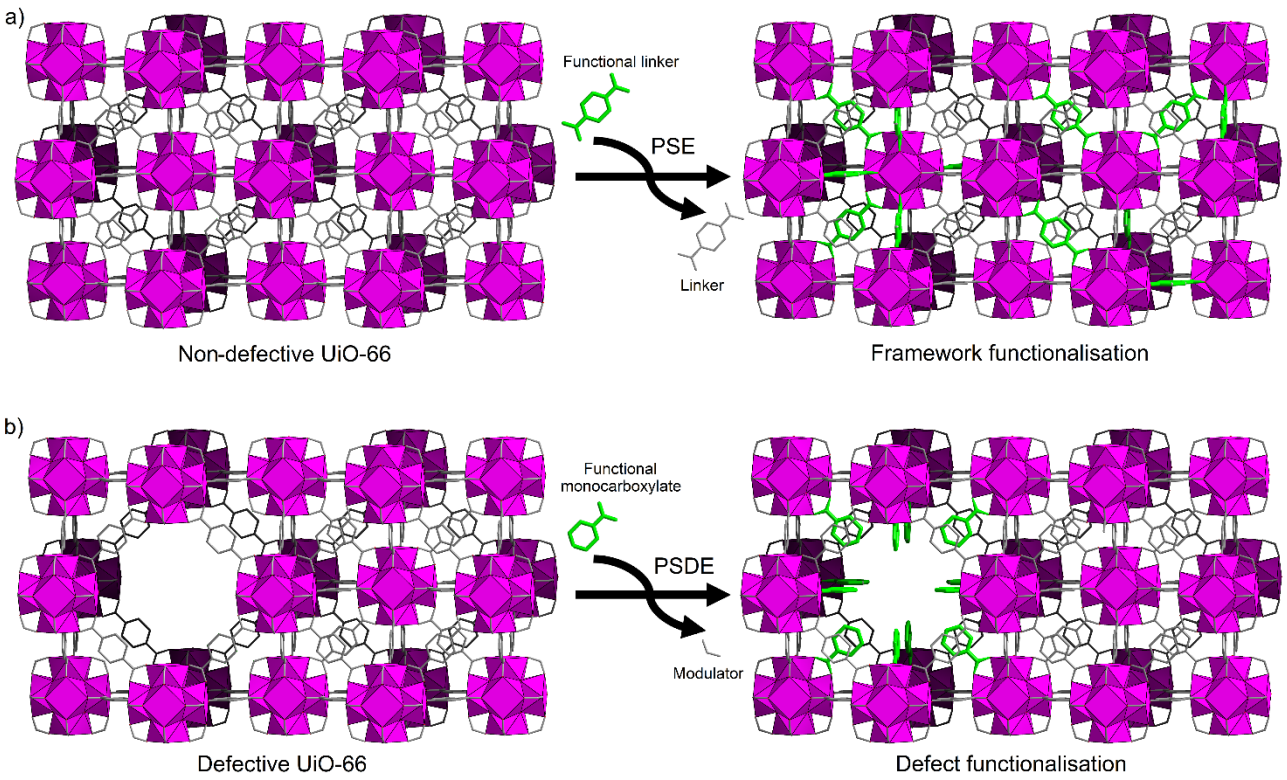

Figure 2. (a) Defect-free UiO-66 undergoes PSE, exchanging one terephthalate linker (represented in grey) with one functional linker (green), which is homogeneously distributed in the structure. (b) UiO-66 containing missing-cluster defects undergoes PSDE, exchanging one modulator unit (grey) with one functional monocarboxylate (green), which is selectively incorporated at defective sites.

Sample preparation and characterization

A batch of FA_mod was solvothermally prepared using BDC linker in the presence of FA as a modulator. The functionalized materials were then synthesized by solid-liquid PSDE, by soaking FA_mod in a solution of the desired acid (Figure 1) in DMF at 80 °C for 24 hours. The structural integrity of the crystalline modified materials was confirmed using PXRD (Figure S1). SEM images do not depict considerable differences, with all the samples displaying the usual octahedral morphology and no evident traces of amorphous matter, corroborating the crystalline nature of the exchanged MOFs (Figures S2-S7). Quantitative NMR analysis of the solids hydrolyzed in alkaline conditions evidenced that FA species grafted at the defective sites of the parental material were almost completely exchanged by benzoic acid analogues (Table 1, Figures S8-S13). In the whole series of materials, the amount of monocarboxylic acid grafted to the defective sites of the parent FA_mod is almost identical. The values of benzoic acid analogue-to-BDC molar ratio fell within a narrow range for all samples from 0.35 to 0.42, allowing us to reliably compare the effect of the grafted species on the sorbents adsorption properties. Using these data, we calculated the average unit cell content for each sample, finding that about 17% of the clusters are missing in these materials, corresponding to about 67% of the unit cells having the **reo** defective topology (see ESI, page S12, for details). TGA shows that substitution of FA with amino-functionalized monocarboxylates slightly decreases the thermal stability of the framework, whereas introduction of BA has no visible effect (Figure S14).

Alongside defect-engineered materials, an almost non-defective UiO-66, prepared with no modulator present during synthesis, No_mod, and functionalized materials resulting from PSE of No_mod with PyDC (No_mod-PyDC) and ABDC (No_mod-ABDC), were synthesized and subsequently characterized. Again, both PXRD (Figure S15) and SEM analysis (Figures S16-S18) do not evidence considerable differences between the starting material and the exchanged MOFs. The degree of linkers exchange lies in a similar range with that observed for defective samples, equaling to 0.33 and 0.32 in No_mod-PyDC and No_mod-ABDC respectively, according to NMR results (Table 1, Figures S19-S21). The incorporation of nitrogen-bearing linkers is further supported by TGA (Figure S22), which shows that decomposition of the framework in No_mod-PyDC

and No_mod-ABDC takes place at lower temperatures, in agreement with previous literature reports.[20, 34, 35]

Table 1. Chemical composition information of the investigated samples

Sample	Benzoic acid analogue/BDC ratio	Proposed formula unit[a]	Average unit cell content[c]	Average unit cell weight (g mol^{-1})
FA_mod	-	$Zr_6O_4(OH)_4(BDC)_{4.92}(FA)_{2.16}$	$Zr_{20.3}O_{13.6}(OH)_{13.6}(BDC)_{16.7}(FA)_{7.3}$	5363.3
FA_mod-NA	0.42	$Zr_6O_4(OH)_4(BDC)_{4.80}(FA)_{0.40}(NA)_{2.00}$	$Zr_{20.0}O_{13.3}(OH)_{13.3}(BDC)_{16.0}(FA)_{1.3}(NA)_{6.7}$	5753.6
FA_mod-PA	0.40	$Zr_6O_4(OH)_4(BDC)_{4.78}(FA)_{0.52}(PA)_{1.92}$	$Zr_{19.9}O_{13.3}(OH)_{13.3}(BDC)_{15.8}(FA)_{1.7}(PA)_{6.4}$	5711.4
FA_mod-BA	0.42	$Zr_6O_4(OH)_4(BDC)_{4.78}(FA)_{0.42}(BA)_{2.02}$	$Zr_{19.9}O_{13.3}(OH)_{13.3}(BDC)_{15.8}(FA)_{1.4}(BA)_{6.8}$	5732.8
FA_mod-ABA	0.35	$Zr_6O_4(OH)_4(BDC)_{4.80}(FA)_{0.70}(ABA)_{1.70}$	$Zr_{20.0}O_{13.3}(OH)_{13.3}(BDC)_{16.0}(FA)_{2.4}(ABA)_{5.7}$	5755.4
FA_mod-AA	0.39	$Zr_6O_4(OH)_4(BDC)_{4.74}(FA)_{0.68}(AA)_{1.84}$	$Zr_{19.9}O_{13.2}(OH)_{13.2}(BDC)_{15.7}(FA)_{2.2}(AA)_{6.0}$	5745.7
Sample	**Functional linker/BDC ratio**	**Proposed formula unit[b]**	**Average unit cell content[c]**	**Average unit cell weight (g mol^{-1})**
No_mod	-	$Zr_6O_4(OH)_4(BDC)_{5.88}(FA)_{0.24}$	$Zr_{24.0}O_{16.0}(OH)_{16.0}(BDC)_{23.5}(FA)_{1.0}$	6612.5
No_mod-PyDC	0.33	$Zr_6O_4(OH)_4(BDC)_{4.50}(PyDC)_{1.47}(FA)_{0.06}$	$Zr_{24.0}O_{16.0}(OH)_{16.0}(BDC)_{18.0}(PyDC)_{5.9}(FA)_{0.2}$	6636.9
No_mod-ABDC	0.32	$Zr_6O_4(OH)_4(BDC)_{4.50}(ABDC)_{1.46}(FA)_{0.08}$	$Zr_{24.0}O_{16.0}(OH)_{16.0}(BDC)_{18.0}(ABDC)_{5.8}(FA)_{0.4}$	6718.8

[a] See Figures S8-13 for details on the calculations to determine the formula unit; [b] See Figures S19-21 for details on the calculations to determine the formula unit; [c] See ESI (pages S12 and S19) for details on the calculations to determine the average unit cell content

Surface area and porosity

Replacement of FA with molecules of higher molecular weight and steric bulk was expected to diminish the porosity and the surface area of the defect-engineered materials. The starting FA_mod has BET surface area of 1520 m^2 g^{-1} and micropore volume of 0.63 cm^3 g^{-1}, owing to the missing clusters defects and the large generated cages present in the material (Figure 3a, Table 2). All the modified defective materials present a BET surface area ranging from 1271 to 1321 m^2 g^{-1}, while their micropore volumes lie between 0.46 and 0.48 cm^3 g^{-1} (Figure 3a, Table 2). Akin porosity properties of the functionalized materials are well anticipated, and they are ascribed to the very close molecular weights and steric bulk of the exchanged acids, and the similar exchange ratios. Nitrogen isotherms in Figure 3a show type 1 sorption behavior, characteristic of microporous materials[36] and are well fitted to the multi-point BET equation in the relative pressure range of 0.001-0.043 (Figure S23).

During PSDE, NA, PA, BA, ABA and AA replace FA occupying bigger pores at the defective sites of the starting material. As it is evident in Figure 3b, functionalized materials exhibit different shape of pore size distribution (PSD) (determined according to NLDFT), when compared to FA_mod, displays two "porosity peaks" corresponding to pores with radius of about 5.5 and 7.5 Å, respectively, with the latter attributed to the presence of missing-cluster defects. The bimodal shape of FA_mod PSD curve is substituted by monomodal distributions for the modified materials presenting a broader "porosity peak" at a half width of 5.5 Å. We hereby applied NLDFT implementing the same kernel in a series of UiO-66 materials prepared in like manner, permitting us to meaningfully compare the obtained results and the shift in pore sizes. A recent study also shows that NLDFT is able to generate reliable pore size distributions in MOFs.[37] In the case of No_mod, no loss of porosity is observed after the exchange of the parental linkers with PyDC (Figure 3c). A slightly decreased porosity in No_mod-ABDC can be justified by the higher molecular weight and steric demand of ABDC. No considerable differences are observed in the PSD curves shape accordingly (Figure 3d). In the case of No_mod, the presence of a minor peak adjacent to the main peak at 6 Å could be due to the presence of a small of amount of defects, probably of missing-linker nature. The BET surface area of 1084 m^2 g^{-1} is however fully consistent with the reported values of non-defective UiO-66.[38]

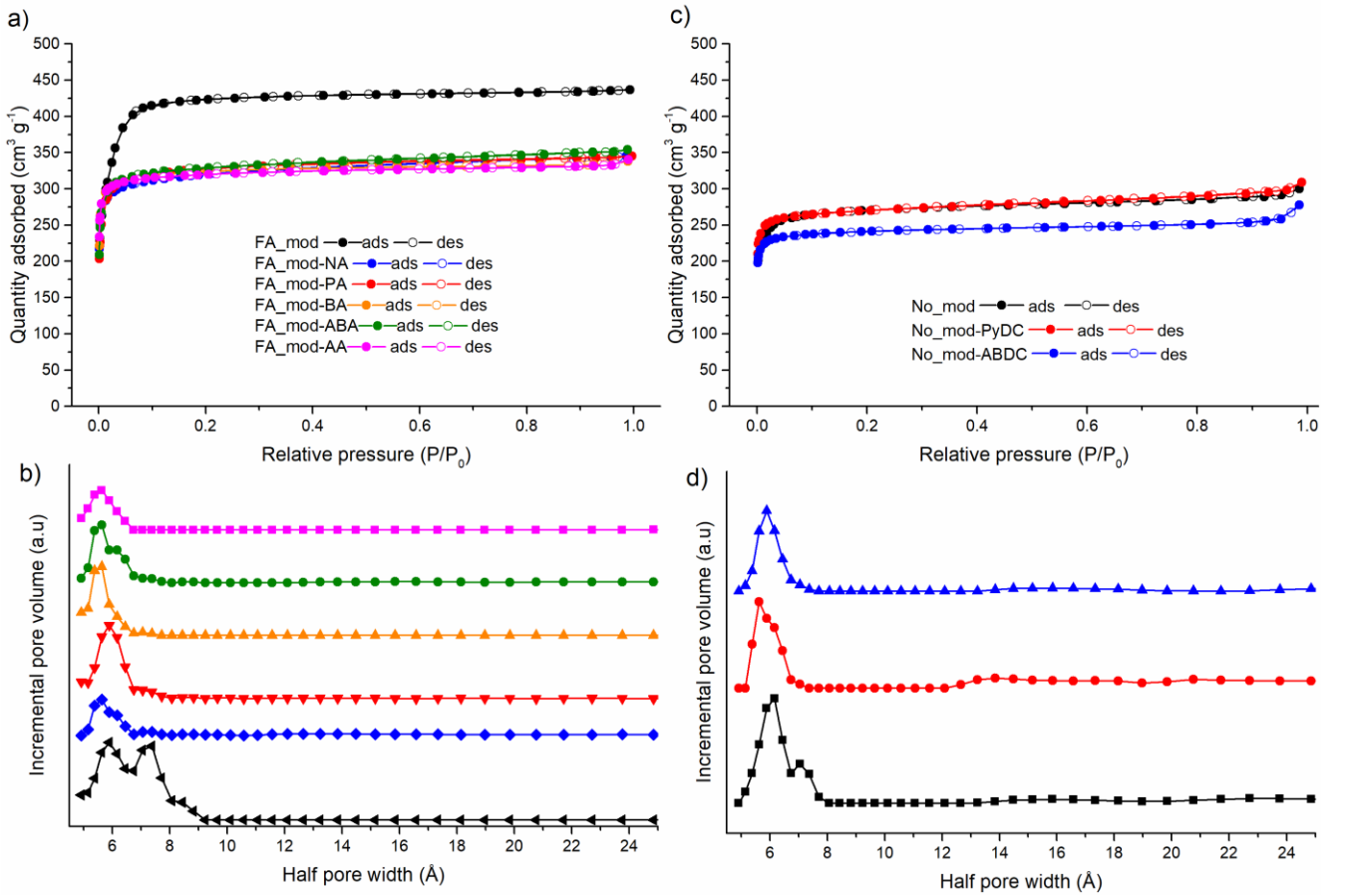

Figure 3. Nitrogen sorption isotherms at 77 K (a) and pore size distribution (b) of FA_mod (black), FA_mod-NA (blue), FA_mod-PA (red), FA_mod-BA (orange), FA_mod-ABA (green) and FA_mod –AA (magenta). Nitrogen sorption isotherm at 77 K (c) and pore size distribution (d) of No_mod (black), No_mod-PyDC (red) and FA_mod-ABDC (blue).

Table 2. Calculated BET Surface area and micropore volume for all the investigated samples.

Sample	BET surface area ($m^2\ g^{-1}$)	Micropore volume ($cm^3\ g^{-1}$)
FA_mod	1520	0.63
FA_mod-NA	1271	0.46
FA_mod-PA	1310	0.48
FA_mod-ABA	1321	0.48
FA_mod-AA	1303	0.48
FA_mod-BA	1313	0.48
Sample	**BET surface area ($m^2\ g^{-1}$)**	**Micropore volume ($cm^3\ g^{-1}$)**
No_mod	1084	0.39
No_mod-PyDC	1090	0.39
No_mod-ABDC	981	0.36

CO_2 capture performance

Successful functionalization of FA_mod by PSDE allows us to assess the relationships between the nature and orientation of the grafted amino groups and the CO_2 sorption capacity. The single component adsorption isotherms of CO_2 were collected at 283, 298 and 313 K up to 10 bar (Figure 4a, Figures S25-S27). As seen in Figure 4c, FA_mod-ABA and FA_mod-AA achieve a CO_2 uptake of 2.14 mol kg^{-1} at 1 bar and 298 K, significantly enhanced (almost 50% higher) compared to the respective uptake of the parent FA_mod that scarcely approaches 1.44 mol kg^{-1}. Changing the amine group position from *ortho* to *meta* (with respect to the carboxylate) does not induce evident differences between the uptake properties of FA_mod-AA and FA_mod-ABA sorbents. FA_mod-NA and FA_mod-PA also display improved sorption behavior towards CO_2, but not as much as the $–NH_2$ containing materials, with both of them presenting an increase of about 25% at atmospheric conditions. Again, changing the amine group from *ortho* to *meta* position (with respect to the carboxylate) does not appear to affect the CO_2 capacity, as in the case of Cu-based MOFs with nitrogen atoms added into the spacers between two terminal isophthalate moieties.[39] Interestingly, introduction of BA in exchange for FA enhances the sorption properties as well. FA_mod-BA shows an uptake of 1.93 mol kg^{-1} at 298 K and 1 bar, accounting for an increase of 34% in comparison with FA_mod. Indeed, pore size engineering has been shown to be an efficient

strategy to improve CO_2 capture in several studies.[40, 41] Grafting of the bulkier BA fills up the large pores present at the defective sites. As a result, CO_2 molecules fit better in the pores, having higher contact areas and consequently stronger van der Waals forces that lead to improved sorption capacity.[16] In the high pressure regime, FA_mod predictably uptakes more than the modified materials, especially at 283 K (Figure S25), as its superior surface area dominates on the capture mechanism and outperforms the enhanced affinity of its counterparts. Converting the uptake values from mol kg^{-1} into molecules of CO_2 per unit cell (molecules/UC) provides additional insight into the performance of the sorbents (Figure 4d, see Page S21 in ESI for details on the conversion procedure). It turns out that FA_mod-ABA and FA_mod-AA are able to accommodate an average of 12.4 molecules/UC at 1 bar and 298 K, corresponding to a 59% improvement, compared with FA_mod, which only uptakes an average of 7.8 molecules/UC.

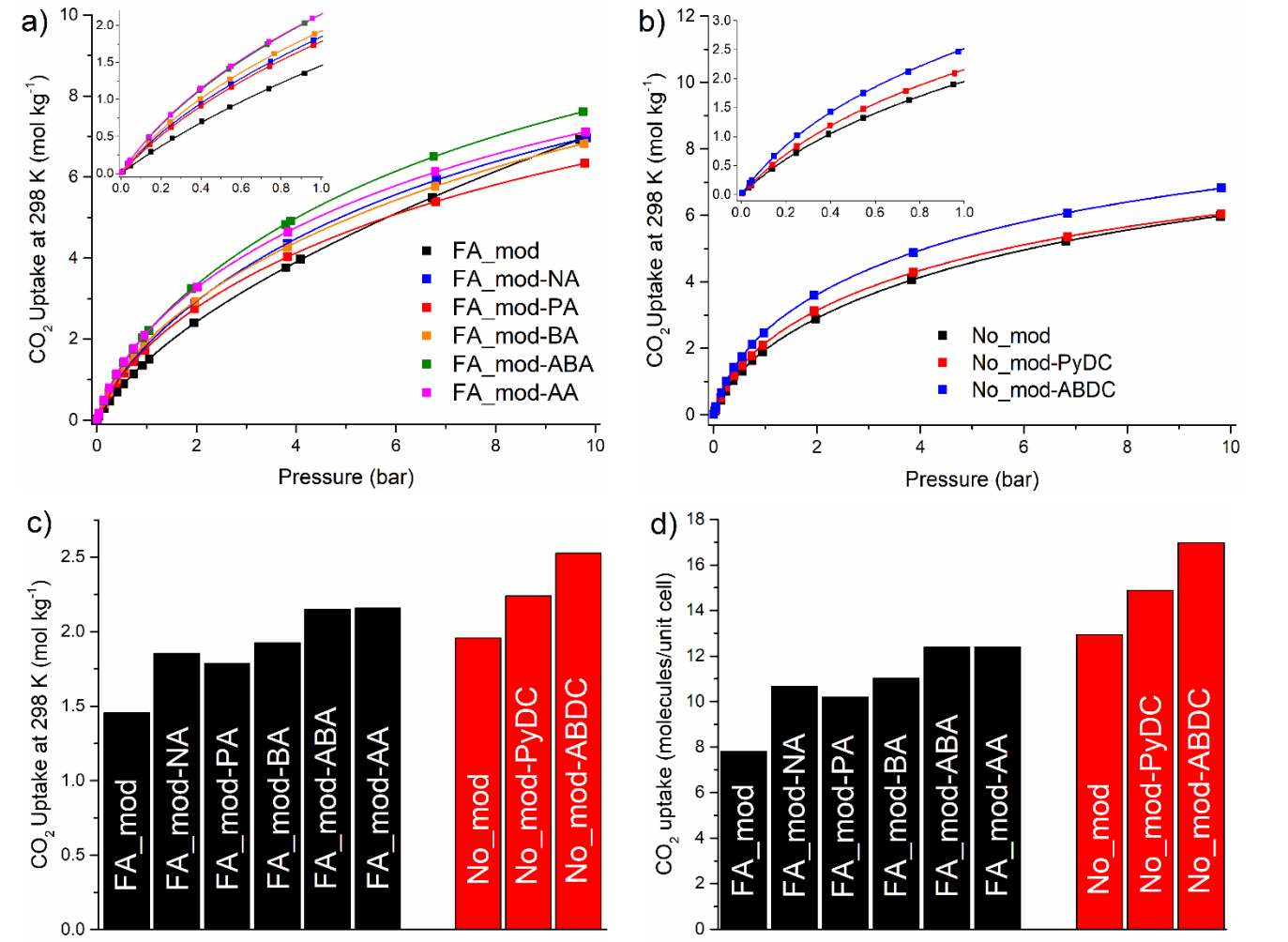

Figure 4. Measured volumetric CO_2 uptakes: (a) CO_2 excess adsorption isotherm at 298 K of FA_mod (black), FA_mod-NA (blue), FA_mod-PA (red), FA_mod-BA (orange), FA_mod-ABA (green) and FA_mod-AA (magenta), (b) CO_2 excess adsorption isotherm at 298 K of No_mod (black), No_mod-PyDC (red), No_mod-ABDC (blue), (c) CO_2 uptake values in mol/kg at 298 K and 1 bar, (d) CO_2 uptake values in molecules/unit cell at 298 K and 1 bar.

Mixed-linker materials also exhibit higher uptakes than No_mod (Figure 4b). Alike defect-engineered materials, the effect of amine group is more pronounced than pyridinic nitrogen, accounting for an increase of 29% in No_mod-ABDC and 10% in No_mod_PyDC at 298 K and 1 bar (Figure 4c). Defect-free No_mod presents higher CO_2 uptake at lower pressures than FA_mod in agreement with the results obtained by Liang et al.,[42] while the defective material is superior at higher pressures. The highest uptake of both the defect-engineered and mixed-linker materials is achieved by No_mod-ABDC. FA_mod-AA exhibits the highest increase of 48%, if compared to the starting material, of all the analyzed MOFs. The uptake values in molecules/UC for the non-defective MOFs suggest that even No_mod is able to accommodate more CO_2 molecules than the best performing defective samples (13 molecules/UC for No_mod, 12.4 molecules/UC for FA_mod-ABA and FA_mod-AA) (Figure 4d). This is probably due to two concurring factors: 1. The removal of about 17% of the hexanuclear Zr clusters in the defective materials, compared to non-defective ones, determines the absence of important adsorption sites. Both experiments and simulations have indeed demonstrated that the -OH groups on the clusters are the main adsorption sites for CO_2.[43] Introduction of benzoic acid analogues at defective sites creates new adsorption sites, which

partially compensate for the loss of the clusters in the defect-engineered materials. 2. Non-defective MOFs feature smaller pores, which, as discussed above, are known to favor interaction of CO_2 with the surface.[16]

The isosteric enthalpy of CO_2 adsorption (IEA) is a common parameter used to estimate the strength of the interaction between CO_2 and the sorbent surface. IEA was calculated from the CO_2 adsorption isotherms at 283, 298 and 313 K using the Clausius-Claperyon equation. All the defect-engineered materials show higher binding energies than FA_mod, as evidenced by the calculated IEA values (Figure 5a). At near-zero loading, the IEA of functionalized sorbents (24-27 kJ mol^{-1}) is significantly higher the starting FA_mod (17.6 kJ mol^{-1}). The improved dispersion interactions is probably the main factor behind the rise in IEA.[44] FA_mod-BA also shows significantly increased IEA, leading us to the conclusion that stronger interaction forces could also be due to structural parameters and not exclusively owed to the nitrogen incorporation. FA_mod-ABA and FA_mod-AA, that capture the highest amount of CO_2, have analogous IEA values to FA_mod-BA, FA_mod-NA and FA_mod-PA, and their superior uptake behavior cannot be directly rationalized by IEA. In agreement with this, moderate IEA values were observed in the channels of a high-performing MOF material lined by basic amine groups and the high CO_2 uptake was not accompanied by strong adsorbent-adsorbate interactions.[45] It appears that, at the degree of functionalization we achieve, IEA does not change significantly. Invoking acid-base properties also does not help in interpreting the observation: the heterocyclic nitrogen atoms in NA (pKa 4.19) and PA (pKa 5.52) are indeed more alkaline than the aromatic amine groups in AA (pKa 3.27) and ABA (pKa 1.25) and should, in principle, be more prone to interact with the weakly acidic carbon atom in the CO_2 molecule. A more lucrative strategy should involve introduction of considerably more basic aliphatic amine groups. One notable feature evident from Figure 4a is that IEA of defect-engineered materials decreases when loading increases from 0.1 to 1 mol kg^{-1}, while IEA of FA_mod remains practically constant over the same loading range. This behavior is likely due to the modification of the pore system and the generation of new adsorption sites, which are preferentially filled at low coverage, upon PSDE. Future computational studies could allow us to gain deeper insight into the interaction between CO_2 and defect-engineered materials. We should also note that error bars of amine functionalized materials and FA_mod-BA overlap, indicating that the difference between the means of IEA is not statistically significant.

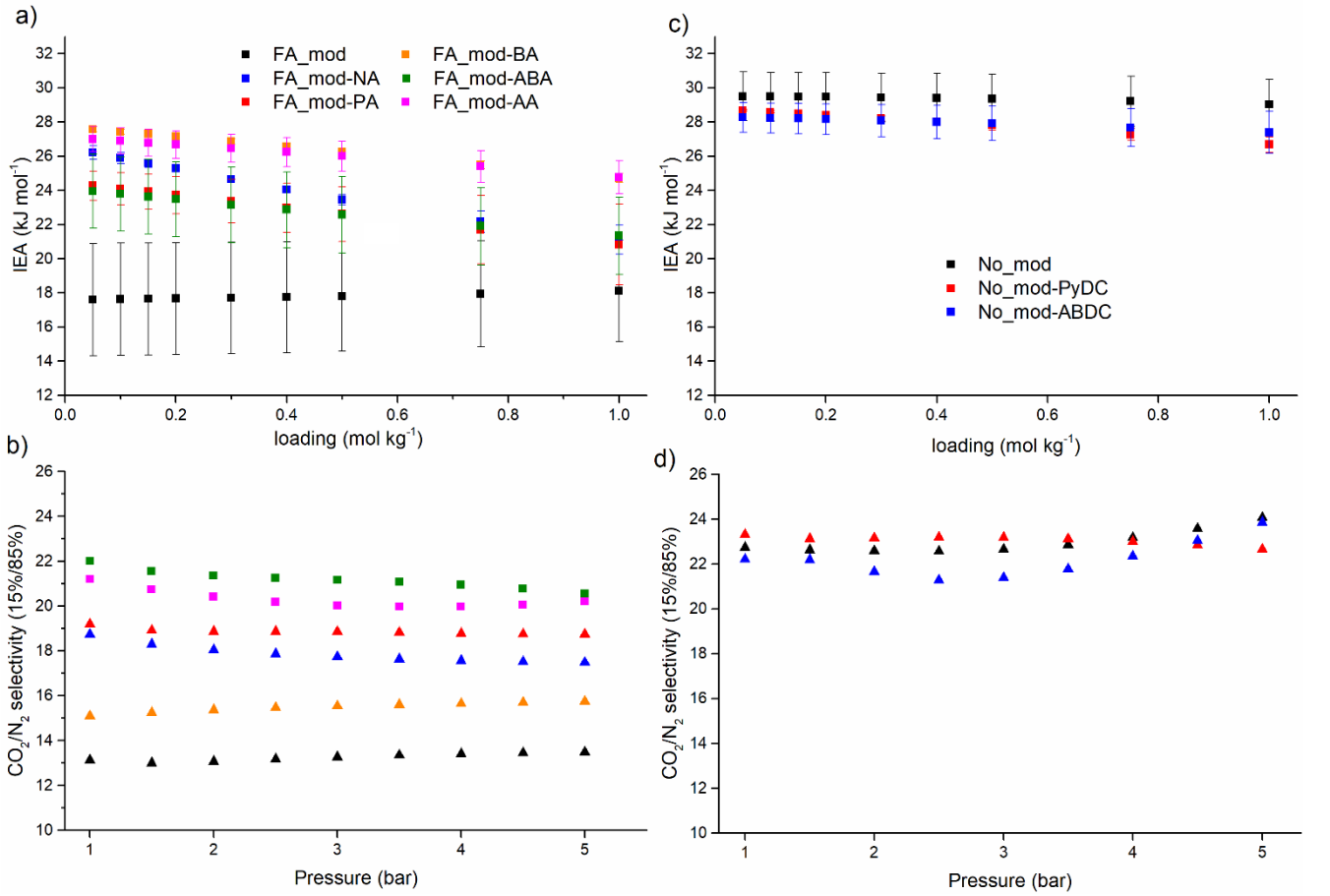

Figure 5. Isosteric enthalpy of CO_2 adsorption as a function of loading (a) and IAST selectivity CO_2 /N_2 (15:85) (b) of FA_mod (black), FA_mod-NA (blue), FA_mod-PA (red), FA_mod-BA (orange), FA_mod-ABA (green) and FA_mod –AA (magenta). Isosteric enthalpy of CO_2 adsorption as a function of loading (c) and IAST selectivity CO_2 /N_2 (15:85) (d) of No_mod (black), No_mod-PyDC (red), FA_mod-ABDC (blue).

CO_2/N_2 selectivity, as determined by the ideal adsorbed solution theory (IAST) for a 0.15:0.85 mixture at 298 K, also appears to increase in the nitrogen functionalized materials, both in pyridine form and amine form (Figure 5b). Following the same pattern of the CO_2 uptake measurements, FA_mod-ABA and FA_MOD-AA have the highest selectivity, achieving a value close to 22, much higher than the value of 14 of FA_mod. Interaction of CO_2 molecules with the amine group via hydrogen bonding or between the N lone pair and the C atom of CO_2, probably cause the enhanced affinity of these materials for CO_2.[44] Notably, the selectivity is barely improved in FA_mod-BA. Given its substantially higher CO_2 uptake, it is inferred that pure pore size engineering could also be favorable for N_2, eventually resulting in a moderate selectivity improvement. This is further supported by the superior N_2 uptake of FA_mod-BA at low pressures (Figure S29).

In the family of non-defective materials, no considerable differences are observed in the values and trends of IEA in the 0.1-1.0 mol kg-1 range of No_mod and its mixed-linker derivatives (Figure 5c). This suggests that the main adsorption sites in these compounds are essentially the same, i.e. the hexanuclear clusters, and that partial functionalization of the framework does not significantly affect the adsorption performance, something that has been instead observed for fully functionalized UiO-66.[18, 20] Again, the basicity of the amine groups does not linearly correlate with the ability to adsorb CO_2: the heterocyclic nitrogen in PyDC has a pKa of 6.46, whereas the aromatic amine group in ABDC has a pKa of 1.12. Similarly, IAST selectivity is practically unchanged upon functionalization (Figure 5d). Overall, the non-defective materials display slightly higher CO_2/N_2 selectivity than the defective materials, probably thanks to their smaller pores. This could partly be explained by the lower porosity of non-defective frameworks: it is known that ultramicropores (5 - 7 Å) are more selective towards CO_2, compared to supermicropores (7 - 20 Å).

Conclusions

The systematic investigation performed in the present study demonstrates that post-synthetic exchange of modulator species grafted at defective sites with various nitrogen-containing monocarboxylates enhances the overall CO_2 capture performance of defective UiO-66. NH_2-functionalized sorbents showed superior performance than the materials bearing heterocyclic nitrogen, although the position of the nitrogen groups did not appear to significantly effect on the gas uptake properties. A CO_2 uptake increase of 48%, compared to the pristine FA_mod, was achieved by defect-functionalized FA_mod-AA at ambient conditions, exceeding the respective value achieved by framework functionalized No_mod-ABDC (29%, compared to No_mod). Notably, the PSDE approach leads to improvement of CO_2/N_2 selectivity, whereas framework functionalization by PSE does not. Simple tailoring of the pore size through exchange of FA with BA also improved the overall CO_2 uptake, but the selectivity improved only fractionally, implying that amino groups are necessary to enhance affinity for CO_2. The successful employment of defect-engineering approach towards enhanced properties unveils the method's potential.

Considering the dynamic and versatile nature of defects in Zr-MOFs, and the variety of guest molecules that could be hosted in larger pores via PSDE, we reveal that our defect-engineering approach entails numerous opportunities for further development as an important tool for tuning the physical-chemical properties of MOFs. Ongoing investigation in our group is aimed at further exploiting PSDE to improve the CO_2 capture performance of defective Zr-MOFs, both introducing functional groups that are not accessible via linker modification in UiO-66, e.g. aliphatic amines, and functionalizing frameworks based on less chemically versatile linkers than BDC.

Conflicts of interest

There are no conflicts to declare.

Acknowledgements

The authors gratefully acknowledge the financial support provided by the Sêr Cymru Chair Programme (A.R.B.). The European Union's Horizon 2020 research and innovation programme under the Marie Skłodowska-Curie grant agreement No 663830 (M.T.), and the Engineering and Physical Sciences Research Council (EPSRC) for funding through the First Grant scheme EP/R01910X/1 (M.T.). The Welsh Government is also acknowledged for the Sêr Cymru II Recapturing Talent Fellowship (E.K.) partly funded by the European Regional Development Fund (ERDF). This work is also part of the Reduce Industrial Carbon Emissions (RICE) and Flexible Integrated Energy Systems (FLEXIS) operations funded by Welsh European Funding Office (WEFO), also partly funded by the ERDF. We would like to acknowledge the assistance provided by the Swansea University AIM Facility, which was funded in part by the EPSRC EP/M028267/1, the ERDF through the Welsh Government grant 80708, and the Sêr Solar project via the Welsh Government. Financial support was also provided the Robert A. Welch Foundation (C-0002).

References

1. *Reducing UK emissions – 2018 Progress Report to Parliament*, CCC, 2018.
2. M. Bui, C. S. Adjiman, A. Bardow, E. J. Anthony, A. Boston, S. Brown, P. S. Fennell, S. Fuss, A. Galindo, L. A. Hackett, J. P.

Hallett, H. J. Herzog, G. Jackson, J. Kemper, S. Krevor, G. C. Maitland, M. Matuszewski, I. S. Metcalfe, C. Petit, G. Puxty, J. Reimer, D. M. Reiner, E. S. Rubin, S. A. Scott, N. Shah, B. Smit, J. P. M. Trusler, P. Webley, J. Wilcox and N. Mac Dowell, *Energy Environ. Sci.*, 2018, **11**, 1062-1176.

3. R. T. J. Porter, M. Fairweather, C. Kolster, N. Mac Dowell, N. Shah and R. M. Woolley, *Int. J. Greenh. Gas Con.*, 2017, **57**, 185-195.
4. A. B. Rao and E. S. Rubin, *Environ. Sci. Technol.*, 2002, **36**, 4467-4475.
5. H. A. Patel, J. Byun and C. T. Yavuz, *ChemSusChem*, 2017, **10**, 1303-1317.
6. Y. Belmabkhout, R. Serna-Guerrero and A. Sayari, *Adsorption*, 2011, **17**, 395-401.
7. D. M. D'Alessandro, B. Smit and J. R. Long, *Angew. Chem. Int. Ed.*, 2010, **49**, 6058-6082.
8. E. S. Sanz-Pérez, C. R. Murdock, S. A. Didas and C. W. Jones, *Chem. Rev.*, 2016, **116**, 11840-11876.
9. K. Sumida, D. L. Rogow, J. A. Mason, T. M. McDonald, E. D. Bloch, Z. R. Herm, T.-H. Bae and J. R. Long, *Chem. Rev.*, 2012, **112**, 724-781.
10. M. H. Alkordi, R. R. Haikal, Y. S. Hassan, A.-H. Emwas and Y. Belmabkhout, *J. Mater. Chem. A*, 2015, **3**, 22584-22590.
11. L. Yichao, K. Chunglong, Z. Qiuju and C. Liang, *Adv. Energy Mater.*, 2017, **7**, 1601296.
12. P. Nugent, Y. Belmabkhout, S. D. Burd, A. J. Cairns, R. Luebke, K. Forrest, T. Pham, S. Ma, B. Space, L. Wojtas, M. Eddaoudi and M. J. Zaworotko, *Nature*, 2013, **495**, 80.
13. C. Wang, X. Liu, N. Keser Demir, J. P. Chen and K. Li, *Chem. Soc. Rev.*, 2016, **45**, 5107-5134.
14. P. M. Bhatt, Y. Belmabkhout, A. Cadiau, K. Adil, O. Shekhah, A. Shkurenko, L. J. Barbour and M. Eddaoudi, *J. Am. Chem. Soc.*, 2016, **138**, 9301-9307.
15. Y. Bai, Y. Dou, L.-H. Xie, W. Rutledge, J.-R. Li and H.-C. Zhou, *Chem. Soc. Rev.*, 2016, **45**, 2327-2367.
16. M. Oschatz and M. Antonietti, *Energy Environ. Sci.*, 2018, **11**, 57-70.
17. S. R. Caskey, A. G. Wong-Foy and A. J. Matzger, *J. Am. Chem. Soc.*, 2008, **130**, 10870-10871.
18. J. Ethiraj, E. Albanese, B. Civalleri, J. G. Vitillo, F. Bonino, S. Chavan, G. C. Shearer, K. P. Lillerud and S. Bordiga, *ChemSusChem*, 2014, **7**, 3382-3388.
19. H. R. Abid, J. Shang, H.-M. Ang and S. Wang, *Int. J. Smart Nano Mater.*, 2013, **4**, 72-82.
20. A. A. Barkhordarian and C. J. Kepert, *J. Mater. Chem. A*, 2017, **5**, 5612-5618.
21. E. Andreoli and A. R. Barron *ChemSusChem*, 2015, **8**, 2635-2644.
22. M. Taddei, *Coord. Chem. Rev.*, 2017, **343**, 1-24.
23. H. Park, S. Kim, B. Jung, M. H. Park, Y. Kim and M. Kim, *Inorg. Chem.*, 2018, **57**, 1040-1047.
24. J. M. Taylor, S. Dekura, R. Ikeda and H. Kitagawa, *Chem. Mater.*, 2015, **27**, 2286-2289.
25. X. Feng, H. S. Jena, K. Leus, G. Wang, J. Ouwehand and P. Van Der Voort, *J. Catal.*, 2018, **365**, 36-42.
26. G. C. Shearer, J. G. Vitillo, S. Bordiga, S. Svelle, U. Olsbye and K. P. Lillerud, *Chem. Mater.*, 2016, **28**, 7190-7193.
27. M. Taddei, R. J. Wakeham, A. Koutsianos, E. Andreoli and A. R. Barron, *Angew. Chem. Int. Ed.*, 2018, **57**, 11706-11710.
28. D. A. Gómez-Gualdrón, P. Z. Moghadam, J. T. Hupp, O. K. Farha and R. Q. Snurr, *J. Am. Chem. Soc.*, 2016, **138**, 215-224.
29. S. Lee, J. H. Lee and J. Kim, *Korean J. Chem. Eng.*, 2018, **35**, 214-221.
30. U. Fluch, V. Paneta, D. Primetzhofer and S. Ott, *Chem. Commun.*, 2017, **53**, 6516-6519.
31. J. A. Boissonnault, A. G. Wong-Foy and A. J. Matzger, *J. Am. Chem. Soc.*, 2017, **139**, 14841-14844.
32. P. Deria, J. E. Mondloch, E. Tylianakis, P. Ghosh, W. Bury, R. Q. Snurr, J. T. Hupp and O. K. Farha, *J. Am. Chem. Soc.*, 2013, **135**, 16801-16804.
33. P. Deria, W. Bury, J. T. Hupp and O. K. Farha, *Chem. Commun.*, 2014, **50**, 1965-1968.
34. S. M. Chavan, G. C. Shearer, S. Svelle, U. Olsbye, F. Bonino, J. Ethiraj, K. P. Lillerud and S. Bordiga, *Inorg. Chem.*, 2014, **53**, 9509-9515.
35. M. Taddei, D. Tiana, N. Casati, J. A. van Bokhoven, B. Smit and M. Ranocchiari, *Phys. Chem. Chem. Phys.*, 2017, **19**, 1551-1559.
36. S. Lowell, Shields, J.E., Thomas, M.A., Thommes, M., *Characterization of Porous Solids and Powders: Surface Area, Pore Size and Density*, Springer Netherlands, 2004.
37. A. Sonnauer, F. Hoffmann, M. Fröba, L. Kienle, V. Duppel, M. Thommes, C. Serre, G. Férey and N. Stock, *Angew. Chem. Int. Ed.*, 2009, **48**, 3791-3794.
38. G. C. Shearer, S. Chavan, S. Bordiga, S. Svelle, U. Olsbye and K. P. Lillerud, *Chem. Mater.*, 2016, **28**, 3749-3761.
39. C. Song, J. Hu, Y. Ling, Y. Feng, R. Krishna, D.-l. Chen and Y. He, *J. Mater. Chem. A*, 2015, **3**, 19417-19426.
40. J. Wang, A. Heerwig, M. R. Lohe, M. Oschatz, L. Borchardt and S. Kaskel, *J. Mater. Chem.*, 2012, **22**, 13911-13913.
41. M. Yiyin, C. Danke, H. Pan, G. Yi, Y. Yulong, Y. Wen and P. Xinsheng, *Chem. Eur. J.*, 2015, **21**, 15127-15132.
42. W. Liang, C. J. Coghlan, F. Ragon, M. Rubio-Martinez, D. M. D'Alessandro and R. Babarao, *Dalton Trans.*, 2016, **45**, 4496-4500.
43. H. Wu, Y. S. Chua, V. Krungleviciute, M. Tyagi, P. Chen, T. Yildirim and W. Zhou, *J. Am. Chem. Soc.*, 2013, **135**, 10525-10532.
44. R. Vaidhyanathan, S. S. Iremonger, G. K. H. Shimizu, P. G. Boyd, S. Alavi and T. K. Woo, *Science*, 2010, **330**, 650-653.
45. S. Nandi, R. Maity, D. Chakraborty, H. Ballav and R. Vaidhyanathan, *Inorg. Chem.*, 2018, **57**, 5267-5272.